J. Fluid Mech. (2003), *vol.* 484, *pp.* 329–346.
DOI: 10.1017/S0022112003004348 Printed in the United Kingdom

Thermally driven reaction fronts in porous media

By T. E. JUPP AND A. W. WOODS

BP Institute for Multiphase Flow, University of Cambridge, Madingley Road, Cambridge, CB3 0EZ, UK

(Received 6 May 2002 and in revised form 27 January 2003)

We examine the reaction fronts that develop when an undersaturated 'injection fluid' displaces a saturated 'formation fluid' in a chemically reactive porous medium. We allow the injection and formation fluids to differ both in temperature and in chemical composition. The undersaturation of the incoming fluid drives a dissolution reaction and leads to the formation of a 'depletion' front. Under certain circumstances, which we describe, the temperature difference drives a separate thermal reaction front. We develop long-time asymptotic solutions of the governing equations which illustrate the interaction between thermal reaction fronts and depletion fronts. Two distinct regimes arise. If the compositional difference between the injection and formation fluids exceeds a critical value, the depletion front travels faster than the thermal front, leaving the porous medium depleted of reactant from the source to a point downstream of the thermal front and no thermal reaction front develops. Conversely, if the compositional difference is smaller than the critical value, a thermal reaction front advances ahead of the depletion front and so there is a double reaction front structure. We illustrate the evolution of the thermal and compositional fields towards these asymptotic solutions with numerical simulations. We discuss the implications of this work for secondary mineralization in subsurface reservoirs.

1. Introduction

There are numerous industrial and natural situations in which fluid of one temperature and composition migrates through a permeable rock, displacing an original fluid of different temperature and composition. Important industrial examples arise in geothermal and hydrocarbon reservoirs. In the geothermal case, warm water or superheated vapour is produced from a subterranean reservoir and replaced by cold water injected by commercial operators. As the cold water migrates through the reservoir, it heats up and displaces the original formation fluid. In hydrocarbon reservoirs, the original formation often contains both water and oil in the pore spaces. As oil is extracted from a producer well, water is typically introduced at an injector well some distance away. There are also natural situations in which fluid of one temperature and composition may flood into an aquifer filled with fluid of a different temperature and composition. Events which might lead to such flooding include earthquakes and changes in sea level. The common feature is that a flow path becomes established between two bodies of water in different thermal and chemical states.

As an intruding fluid moves through a porous matrix, minerals in solution in the fluid may become undersaturated or supersaturated as a result of changes in

temperature and pressure, leading to dissolution or precipitation reactions which act to restore the system to equilibrium (Phillips 1991). In the geothermal and hydrocarbon industries, important precipitation reactions include the formation of calcium carbonate, silica and barium sulphate. In a geological context, the dolomitization of limestone can occur when magnesium-rich seawater percolates through a formation previously flooded with fresh water. There is considerable interest in the dynamics of these reactions since the associated changes in permeability may change the pattern and rate of fluid flow through the rock.

When fluid is injected into a porous layer at a different temperature, a thermal front develops across which the temperature of the fluid adjusts to that of the formation. This thermal front travels more slowly than the fluid itself, since the fluid advances through the pore space alone, while the thermal signal must propagate through the grains of the porous medium as well (Phillips 1991; Woods & Fitzgerald 1993). As the injected fluid travels across this temperature front, the solubility of dissolved minerals changes, and this may lead to precipitation or dissolution and the formation of a thermal reaction front.

Thermal reaction fronts are quite distinct from the depletion fronts which develop when undersaturated fluid is injected into a porous layer. In the case of depletion fronts, the advancing fluid dissolves some of the mineral in the formation to restore the fluid to chemical equilibrium, and thereby depletes the formation of mineral near the source of fluid. Phillips (1991) and Hinch & Bhatt (1990) show how these depletion fronts can be modelled mathematically by considering the conservation of mass and a reaction law controlling the kinetics of the reaction.

In comparison with depletion fronts, thermal reaction fronts have received relatively little attention. The main purpose of this work is to develop a model for thermal reaction fronts, and to explore how they interact with depletion fronts when fluid is injected into a reactive porous layer. First, we develop a theoretical model of the reactions which arise when an injection fluid displaces a formation fluid of different composition and temperature. Secondly, we develop long-time asymptotic solutions which determine the conditions under which thermal reaction fronts form. Thirdly, we use numerical simulations to illustrate the evolution of the system from the first injection of the fluid to the long-time asymptotic state. Finally, we consider the implications of our work for the injection of water in both geothermal and hydrocarbon reservoirs.

Our model concerns a simple displacement flow rather than a multi-phase flow in which the two fluids are simultaneously present but flow at different rates. Flows of the latter type, which are considerably more complicated, are considered in similar contexts by Fayers (1962), Karakas, Saneie & Yortsos (1986), deZabala *et al.* (1982) and deZabala & Radke (1986).

2. The governing equations

We consider the displacement of a formation fluid in a semi-infinite, one-dimensional porous medium occupying the half-space $x \geqslant 0$ (figure 1). The porous medium is filled initially with a formation fluid which is in thermal and chemical equilibrium, and fluid motion begins at time $t = 0$. For later times $t > 0$, the injection fluid is introduced at $x = 0$ with constant Darcy velocity u in the x-direction.

We suppose that the porous medium contains a single chemically reactive species. This species can exist either in the solid state on the grains of the porous medium, or as a solute in the injection and formation fluids. The amount of reactive species in

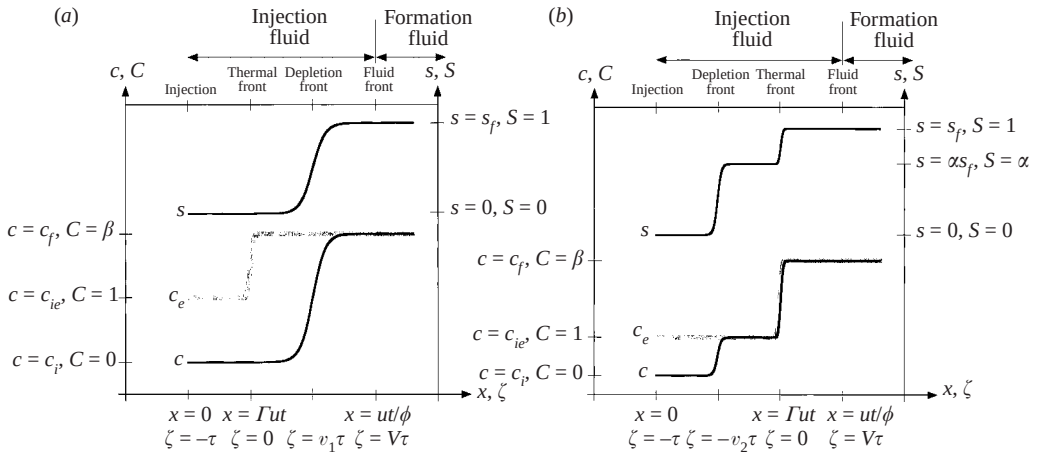

FIGURE 1. Sketch showing typical solutions at a time t after the injection fluid is first introduced. Variables are defined in the text. (*a*) A single reaction front solution in which the thermal front travels upstream of the depletion front. Fluid concentration c, equilibrium concentration c_e and solid concentration s are shown. (*b*) A double reaction front solution in which the thermal front travels downstream of the depletion front.

the solid state is expressed by the 'solid concentration' $s(x,t)$ which has dimensions of moles of solid reactant per unit volume of solid. It follows that unit volume of the fluid-filled porous medium contains $(1-\phi)s$ moles of reactant in the solid state, where ϕ is the porosity. The initial solid concentration in the formation is $s(x,0) = s_f$. Similarly, the amount of reactant dissolved in the fluid is expressed by the 'fluid concentration' $c(x,t)$ which has dimensions of moles of reactant in solution per unit volume of fluid. It follows that unit volume of the fluid-filled porous medium contains ϕc moles of dissolved reactant. The initial fluid concentration in the formation is $c(x,0) = c_f$.

We now consider the equilibrium concentration $c_e(x,t)$ of the dissolved reactant, which has the same dimensions as the true concentration c. Since the formation fluid is assumed to be in equilibrium initially, it follows that $c_e(x,0) = c(x,0) = c_f$. In general, the equilibrium concentration is a function of the temperature and pressure of the fluid. Specifically, the equilibrium concentration is given by (Nordstrom & Munoz 1994)

$$c_e = c_{e0} \exp\left(\frac{-\Delta G_r}{RT}\right), \tag{2.1}$$

where $R = 8.3\,\mathrm{J\,mol^{-1}\,K^{-1}}$ is the gas constant, T is the temperature in Kelvin and $\Delta G_r(p,T)$ is the Gibbs free energy of solution at pressure p and temperature T. The Gibbs free energy in equation (2.1) is calculated relative to that of a solution at the reference concentration c_{e0}. For example, in the case of silica at 1 bar and 25 °C, Nordstrom & Munoz (1994) quote a value $\Delta G_r = 22.7\,\mathrm{kJ\,mol^{-1}}$ with respect to a '1 molal reference concentration' (corresponding to $c_{e0} = 1000\ \mathrm{mol\,m^{-3}}$ in our volumetric concentration units). For simplicity, we shall assume that the equilibrium concentration is independent of pressure and that the temperature range is sufficiently small that equation (2.1) can be approximated by a linear relationship of the form $c_e = a + bT$. For a prograde mineral such as silica, $\Delta G_r > 0$ and so $b > 0$ (Manning 1994), while for a retrograde mineral such as anhydrite, $\Delta G_r < 0$ and so $b < 0$

(Bowers, Jackson & Helgeson 1984). In the analysis below we derive a solution which applies equally to prograde and retrograde minerals.

2.1. *The evolution of temperature and equilibrium concentration*

We now consider the evolution of the system when the formation fluid at temperature T_f and concentration c_f is displaced by the injection fluid at temperature T_i and concentration c_i. Phillips (1991, § 2.8) shows that the evolution of temperature is controlled by an advection–diffusion equation of the form

$$\frac{\partial T}{\partial t} + \frac{(\rho c_p)_l}{\phi(\rho c_p)_l + (1-\phi)(\rho c_p)_s} u \frac{\partial T}{\partial x} = D_T \frac{\partial^2 T}{\partial x^2} + Q_H, \tag{2.2}$$

where D_T is the effective thermal diffusivity of the fluid-filled porous medium, taking account of both molecular diffusion and macroscopic dispersion. The quantity $(\rho c_p)_l$ is the volumetric heat capacity of the fluid, $(\rho c_p)_s$ is the volumetric heat capacity of the solid grains of the porous medium and Q_H is the volumetric rate of heat production by chemical reactions.

We now consider whether the heat produced or absorbed by chemical reactions (Q_H) is significant in the thermal balance. A typical enthalpy of dissolution is at most of order $100\,\mathrm{kJ\,mol^{-1}}$, while typical aqueous concentrations are at most of order $10^{-3}\,\mathrm{mol\,kg^{-1}}$ (Nordstrom & Munoz 1994). Since the heat capacity of water is $4.2\,\mathrm{kJ\,kg^{-1}\,K^{-1}}$ we expect the temperature change due to reactions to be at most of order 0.02 K. This is much smaller than the temperature difference $(T_f - T_i)$ of between 1 K and 100 K which we envisage between the formation and injection fluids. Consequently, we make the approximation $Q_H = 0$. By restricting attention to this regime in which the chemistry has a negligible effect on the temperature, we are able to decouple the thermal field from the compositional field.

Returning to equation (2.2), we define the dimensionless number

$$\Gamma = \frac{(\rho c_p)_l}{\phi(\rho c_p)_l + (1-\phi)(\rho c_p)_s}$$

which measures the advective propagation speed of thermal signals as a fraction of the Darcy velocity. Since it is assumed that $c_e = a + bT$, equilibrium concentration can be used as a proxy for temperature, and all thermal effects can be described in terms of the attendant change in equilibrium concentration c_e. Accordingly, equation (2.2) can be rewritten as

$$\frac{\partial c_e}{\partial t} + \Gamma u \frac{\partial c_e}{\partial x} = D_T \frac{\partial^2 c_e}{\partial x^2}. \tag{2.3}$$

This equation admits front-like solutions associated with changes in temperature and we shall refer to these as 'thermal fronts'. Thermal fronts propagate at speed Γu and spread at a rate governed by the effective thermal diffusivity D_T. In the cases where the thermal front drives a reaction, the associated fronts in the fluid and solid concentrations will be labelled 'thermal reaction fronts'. The equilibrium concentration of the injection fluid is $c_{ie} = a + bT_i$. Since we require the injection fluid to be undersaturated, it follows that $c_i \leqslant c_{ie}$. The formation fluid is saturated initially, so equation (2.3) must be solved subject to the initial condition $c_e(x, 0) = c_f$ and the boundary condition $c_e(0, t) = c_{ie}$ for $t > 0$.

2.2. *The evolution of fluid concentration and solid concentration*

We now consider the chemical transfer of a mineral species between the porous medium and the fluid. Our approach mirrors that of Phillips (1991, § 4.3). We assume

that the rate of transfer of reactant from the porous medium to the fluid takes the form

$$Q_C = \phi k \left(\frac{s}{s_f}\right)(c_e - c)H(s). \tag{2.4}$$

The purpose of the Heaviside function

$$H(s) = \begin{cases} 0, & s \leqslant 0 \\ 1, & s > 0 \end{cases}$$

in equation (2.4) is to ensure that the unphysical regime $s < 0$ does not occur. The parameter k is a reaction rate constant with dimensions of reciprocal time and Q_C has dimensions of moles of reactant per unit volume of fluid-filled porous medium per unit time. The rate law of equation (2.4) expresses the idea that we expect the rate of reaction to increase with the amount of solid reactant present on the grains of the porous medium s, and with the degree of disequilibrium of the fluid $(c_e - c)$.

In a real system, the reaction rate constant k is expected to depend on temperature via an Arrhenius equation (Lasaga 1998) of the form

$$k(T) = \left[k_r \exp\left(\frac{E_a}{RT_r}\right)\right] \exp\left(\frac{-E_a}{RT}\right), \tag{2.5}$$

where E_a is the activation energy of the reaction and the reaction rate takes the value k_r at the reference temperature T_r. Lasaga (1984) suggests that an activation energy $E_a = 60\,\mathrm{kJ\,mol^{-1}}$ may be considered typical for mineral–water reactions.

In our model, we assume for simplicity that the reaction rate is independent of temperature. This is valid if the change in temperature across the reaction front ΔT is small compared to the absolute temperature T. Thus, when $\Delta T/T \ll 1$, the fractional change in reaction rate associated with the thermal front is small. The assumption of a constant reaction rate allows us to derive some simple analytical solutions which give insight into the interaction of thermal and compositional fronts. We shall then consider the effect that a temperature-dependent reaction rate would have on these solutions.

Phillips (1991, § 2.9) shows that the fluid concentration is controlled by an advection–diffusion-reaction equation of the form

$$\frac{\partial c}{\partial t} + \left(\frac{u}{\phi}\right)\frac{\partial c}{\partial x} = D_C \frac{\partial^2 c}{\partial x^2} + \frac{Q_C}{\phi}, \tag{2.6}$$

where D_C is the effective compositional diffusivity, taking account of both molecular diffusion and macroscopic dispersion. Thus, in the absence of reactions ($Q_C = 0$), there is a 'fluid front' separating the injection fluid from the formation fluid, which travels at the interstitial fluid speed u/ϕ and spreads under dispersion and diffusion.

The concentration of reactant in the solid changes because of chemical transfer from the fluid. To allow for the stoichiometry of the reaction, we suppose that ν moles of dissolved reactant are required to react fully with one mole of solid reactant. Consequently, a change δc in the fluid concentration leads to a change $\delta s = -\phi \delta c/\nu(1-\phi)$ in the solid concentration. The solid concentration is therefore governed by the equation

$$\frac{\partial s}{\partial t} = -\frac{Q_C}{(1-\phi)\nu}. \tag{2.7}$$

2.3. *Dimensionless form of the governing equations*

It is useful to recast the governing equations (2.3), (2.6) and (2.7) in dimensionless form. The thermal front migrates with speed Γu, and so we introduce the dimensionless coordinates

$$\zeta = \frac{\Gamma u}{D_T}(x - \Gamma u t), \quad \tau = \frac{\Gamma^2 u^2}{D_T} t, \tag{2.8}$$

and the dimensionless concentrations

$$C(\zeta, \tau) = \frac{c - c_i}{c_{ie} - c_i}, \quad C_E(\zeta, \tau) = \frac{c_e - c_i}{c_{ie} - c_i}, \quad S(\zeta, \tau) = \frac{s}{s_f}. \tag{2.9}$$

We stress that the dimensionless position ζ moves with respect to the dimensional position x so that the point of fluid injection $x = 0$ is given in dimensionless terms by $\zeta = -\tau$.

It follows from equations (2.3), (2.4), (2.6) and (2.7) that the evolution of the system is governed by the dimensionless system of equations

$$\frac{\partial C_E}{\partial \tau} = \frac{\partial^2 C_E}{\partial \zeta^2}, \tag{2.10}$$

$$\frac{\partial C}{\partial \tau} + V \frac{\partial C}{\partial \zeta} = \epsilon \frac{\partial^2 C}{\partial \zeta^2} + PS(C_E - C), \tag{2.11}$$

$$\frac{\partial S}{\partial \tau} - \frac{\partial S}{\partial \zeta} = -\lambda PS(C_E - C), \tag{2.12}$$

with initial conditions

$$C_E(\zeta, 0) = C(\zeta, 0) = \beta \quad \text{and} \quad S(\zeta, 0) = 1 \quad \text{for} \quad \zeta \geqslant 0, \tag{2.13}$$

and boundary conditions

$$C_E(-\tau, \tau) = 1 \quad \text{and} \quad C(-\tau, \tau) = 0 \quad \text{for} \quad \tau > 0. \tag{2.14}$$

The five dimensionless parameters which control the system are

$$V = \frac{1 - \phi\Gamma}{\phi\Gamma}, \quad P = \frac{kD_T}{\Gamma^2 u^2}, \quad \lambda = \frac{\phi(c_{ie} - c_i)}{s_f(1 - \phi)\nu}, \quad \beta = \frac{(c_f - c_i)}{(c_{ie} - c_i)}, \quad \epsilon = \frac{D_C}{D_T}. \tag{2.15}$$

The parameter V is the dimensionless speed of the fluid front in relation to the thermal front (figure 1), while the parameter P is a dimensionless reaction rate. The governing equations show that chemical reaction occurs over a timescale $1/k$, while the thermal front becomes established on a timescale $D_T/\Gamma^2 u^2$. (This is the value of time t for which the thermal front has been advected a distance Γut which exceeds the distance $\sqrt{D_T t}$ that it has spread under dispersion and diffusion.) Thus, P is the ratio of the timescale of formation of the thermal front ($D_T/\Gamma^2 u^2$) to the timescale over which reactions occur ($1/k$). The parameter λ is a measure of the undersaturation $c_{ie} - c_i$ of the injection fluid which tends to remove solid reactant from the rock. Specifically, λ is the ratio of the maximum amount of solid reactant which could be removed by this reaction per unit volume $\phi(c_{ie} - c_i)/\nu$ to the amount of solid reactant initially present on the rock per unit volume $(1 - \phi)s_f$. The parameter β is the ratio of the difference in composition of the injection and formation fluids to the undersaturation of the injection fluid. Finally, ϵ is a 'reciprocal Lewis number' giving the ratio of the effective solutal and thermal diffusivities. Typically, $\epsilon \ll 1$, and solutal

diffusion can be neglected. For illustrative purposes, we shall assume that $\epsilon = 0.01$ in our simulations.

We note that P is the only dimensionless parameter that depends on the reaction rate k. It follows that any temperature dependence of the reaction rate in equation (2.5) could influence the solution only via the rate parameter P. Accordingly, we shall derive solutions under the assumption that P is constant and then consider qualitatively the effect that a temperature-dependent P would have on these solutions.

3. Asymptotic solutions of the equations at large times

Ogata & Banks (1961) give an exact solution of equation (2.10) with conditions (2.13) and (2.14):

$$C_E(\zeta, \tau) = 1 + (\beta - 1)\frac{1 + \operatorname{erf}\left(\zeta/2\tau^{1/2}\right) - \operatorname{erfc}\left((\zeta + 2\tau)/2\tau^{1/2}\right)\exp(\zeta + \tau)}{2}, \quad (3.1)$$

where

$$\operatorname{erf}(x) = \frac{2}{\sqrt{\pi}}\int_0^x \exp(-y^2)\,\mathrm{d}y \text{ and } \operatorname{erfc}(x) = 1 - \operatorname{erf}(x).$$

Since $\operatorname{erfc}(x) \sim (1/\sqrt{\pi})x^{-1}\exp(-x^2)$ as $x \to \infty$, the final term can be approximated at long times, and we can obtain

$$C_E(\zeta, \tau) \approx 1 + (\beta - 1)\frac{1 + \operatorname{erf}\left(\zeta/2\tau^{1/2}\right)}{2}, \quad \tau \gg 1, \quad (3.2)$$

which corresponds to a thermal front localized about $\zeta = 0$. The condition $\tau \gg 1$ in equation (3.2) reflects the fact that the thermal front becomes established over a dimensionless timescale of order unity. We note that the equilibrium concentration (or equivalently, the temperature) is known exactly for all times and evolves independently of any chemical reactions. This is a result of our assumption that the thermal effect of reactions (the term Q_H in equation (2.2)) is negligible.

Before considering the evolution of the fluid and solid concentrations, it is useful to recognize that two distinct types of solution may be expected depending on the relative speeds of the thermal front and the depletion front (figure 1). The change in equilibrium concentration across the thermal front tends to drive a reaction between the fluid and the rock. No such thermal reaction front can form, however, if the porous medium has already been depleted of reactant by the passage of the depletion front. Thus, if the depletion front moves faster than the thermal front, we expect a single reaction front solution with no thermal reaction front (figure 1*a*). Conversely, if the depletion front moves more slowly than the thermal front, we expect a double reaction front solution in which a thermal reaction front develops in addition to the depletion front (figure 1*b*).

To determine the conditions under which each of these regimes arises, we present a solution for the case of a single reaction front, and compare the calculated speed of this depletion front with the speed of the thermal front. We then develop an asymptotic solution for the case of a double reaction front where the thermal front moves faster than the depletion front and leads to the formation of a thermal reaction front.

3.1. *Single reaction front solutions*

We now find asymptotic solutions to equations (2.11) and (2.12) in the case where the depletion front travels downstream of the thermal front as in figure 1(*a*). Following

Phillips (1991) we expect the depletion front to be described by travelling wave solutions of the form $C(\zeta - v_1\tau)$, $S(\zeta - v_1\tau)$, where $v_1 > 0$ to ensure that the depletion front front lies downstream of the thermal front. The boundary conditions are $C = S = 0$ for $\zeta = -\tau$ and $C \to \beta$, $S \to 1$ as $\zeta \to \infty$. The asymptotic solution at long times is

$$C = \frac{\beta}{1 + \exp(-\omega_1(\zeta - v_1\tau))}, \quad S = \frac{1}{1 + \exp(-\omega_1(\zeta - v_1\tau))}. \tag{3.3}$$

Direct substitution yields

$$v_1 = \left(\frac{\lambda\beta(1+V)}{(1+\lambda\beta)} - 1\right), \quad \omega_1 = \frac{P(1+\lambda\beta)}{1+V}. \tag{3.4}$$

Our assumption that $v_1 > 0$ implies the condition

$$\lambda V\beta > 1 \tag{3.5}$$

for this single reaction front solution to be valid. In physical terms, this is equivalent to the condition

$$c_f - c_i > s_f \frac{(1-\phi)\Gamma\nu}{1-\phi\Gamma}. \tag{3.6}$$

We deduce that a single reaction front of the depletion type will occur if (i) the difference in concentration between the formation and injection fluids is sufficiently large; (ii) the concentration of the reactant on the rock is sufficiently small; or (iii) the speed of the thermal front is sufficiently small. Furthermore, we deduce that if the injected fluid has a greater concentration than the original formation fluid ($c_i > c_f$) then this single front structure is impossible and a double front structure must develop. For example, in the case of a prograde mineral, it would be possible to have $c_i > c_{ie} > c_f$ if the injection fluid were much hotter than the formation fluid. Conversely, if the injected liquid has a lower concentration than the formation fluid ($c_i < c_f$), then either a single reaction front or a double reaction front may develop, depending on whether inequality (3.6) is satisfied.

3.2. *Double reaction front solutions*

We now consider the nature of the solution in the case where the thermal front travels faster than the depletion front as in figure 1(*b*). We derive separate asymptotic solutions in the region of the thermal front and in the region of the depletion front.

3.2.1. *Depletion front*

As in § 3.1, the depletion front is governed by equations (2.11) and (2.12) and we expect travelling wave solutions of the form $C(\zeta + v_2\tau)$, $S(\zeta + v_2\tau)$, with the restriction that $v_2 > 0$ so that the depletion front lies upstream of the thermal front. Far upstream of the depletion front ($\zeta \ll -v_2\tau$) we require $C = 0$ and $S = 0$. Conversely, in the region between the thermal front and the depletion front ($-v_2\tau \ll \zeta \ll 0$) we require $C = 1$ and we set $S = \alpha$. The constant α will be determined in § 3.2.2 from consideration of the thermal reaction front. The asymptotic solution at long times is then seen to be

$$C = \frac{1}{1 + \exp(-\omega_2(\zeta + v_2\tau))}, \quad S = \frac{\alpha}{1 + \exp(-\omega_2(\zeta + v_2\tau))}, \tag{3.7}$$

by analogy with § 3.1. Direct substitution yields

$$v_2 = 1 - \frac{\lambda(1+V)}{\lambda+\alpha}, \quad \omega_2 = \frac{P(\lambda+\alpha)}{1+V}. \tag{3.8}$$

Our assumption that $v_2 > 0$ implies the condition

$$\frac{\lambda V}{\alpha} < 1 \tag{3.9}$$

for this double reaction front solution to be valid.

3.2.2. *Thermal reaction front*

We now solve for the reaction which develops across the thermal front. It is useful to define the dimensionless coordinate

$$\eta = \frac{\zeta}{2\sqrt{\tau}}, \tag{3.10}$$

so that equation (3.2) can be written as

$$C_E(\eta, \tau) \approx f_0(\eta), \quad \tau \gg 1, \tag{3.11}$$

where

$$f_0(\eta) = 1 + (\beta - 1)\frac{1 + \mathrm{erf}(\eta)}{2}. \tag{3.12}$$

It can be shown that

$$\frac{\mathrm{d}^2 f_0}{\mathrm{d}\eta^2} = -2\eta \frac{\mathrm{d} f_0}{\mathrm{d}\eta}. \tag{3.13}$$

The governing equations (2.11) and (2.12) become

$$\frac{\partial C}{\partial \tau} + \tfrac{1}{2}\left(V\tau^{-1/2} - \eta\tau^{-1}\right)\frac{\partial C}{\partial \eta} - \tfrac{1}{4}\epsilon\tau^{-1}\frac{\partial^2 C}{\partial \eta^2} + PS(C - C_E) = 0, \tag{3.14}$$

$$\frac{\partial S}{\partial \tau} + \tfrac{1}{2}\left(-\tau^{-1/2} - \eta\tau^{-1}\right)\frac{\partial S}{\partial \eta} - \lambda PS(C - C_E) = 0. \tag{3.15}$$

For sufficiently long times the boundary conditions (2.13) and (2.14) can be approximated by $S = 1$, $C = \beta$ for $\eta \gg 0$ and $S = \alpha$, $C = 1$ for $\eta \ll 0$. We seek an asymptotic solution of the form

$$C(\eta, \tau) = \sum_{n=0}^{\infty} f_n(\eta)\,\tau^{-n/2}, \quad S(\eta, \tau) = \sum_{n=0}^{\infty} g_n(\eta)\,\tau^{-n/2}. \tag{3.16}$$

Substitution into the governing equations (3.14) and (3.15), use of the relation (3.13) and matching powers of τ can be used to yield the sets of functions $\{f_n(\eta)\}$ and $\{g_n(\eta)\}$ (see the Appendix). The leading-order terms $f_0(\eta)$ and $g_0(\eta)$ give the asymptotic solution

$$C = C_E, \quad S = 1 + \lambda V(C_E - \beta), \tag{3.17}$$

which is valid at long times. Evaluating equation (3.17) for S at long times in the region $\eta \ll 0$, we deduce that

$$\alpha = 1 + \lambda V(1 - \beta). \tag{3.18}$$

Combining this with the solution for the depletion front (equation (3.8)), we find that

$$v_2 = 1 - \frac{\lambda(1 + V)}{1 + \lambda + \lambda V(1 - \beta)}, \quad \omega_2 = \frac{P(1 + \lambda + \lambda V(1 - \beta))}{1 + V}, \tag{3.19}$$

and so the critical case in which $v_2 = 0$ and the thermal and depletion fronts overlap is given by

$$\lambda V\beta = 1, \tag{3.20}$$

which is consistent with inequality (3.5) derived from the analysis of a single reaction front.

4. Summary of the different asymptotic solutions

The analysis above shows that several qualitatively different solutions may arise depending on the change in equilibrium concentration across the thermal front and the degree of undersaturation of the injected fluid. We now describe the range of possible asymptotic solutions and illustrate our discussion with figures 2 and 3. In each case shown in these figures, the left-hand diagram shows the asymptotic solution profiles while the right-hand diagram shows the path of a fluid particle in (c_e, c)-space as it moves through the formation. The left- and right-hand diagrams can be interpreted in tandem by bearing in mind that a fluid particle always travels faster than any of the reaction fronts. Specifically, we consider a fluid particle injected at $x = 0$ (or $\zeta = -\tau$) in an initial state in which $c_e = c_{ie}$ and $c = c_i$. After it has flowed past any fronts ($\zeta \gg V\tau$) it achieves a final state in which $c_e = c_f$ and $c = c_f$. The changes in state associated with the particle's passage through the fronts are seen as the step-changes in the profiles of c_e and c in the left-hand diagrams. In terms of the right-hand diagrams, the fluid particle's motion past the fronts is represented by a path through state-space from the initial point (c_{ie}, c_i) to the final point (c_f, c_f).

If the injection fluid has a greater equilibrium concentration than the formation fluid ($\beta < 1$) then there are three types of solution as shown in figure 2. First, when the injection fluid has a concentration in excess of the formation fluid ($\beta < 0$), a double front structure develops for all values of λ as shown in § 3.1. A depletion front is formed upstream of the thermal front (figure 2*a*). The fluid returns to equilibrium across this depletion front, and then advances to the thermal front, across which it reaches the formation temperature and maintains chemical equilibrium by precipitating. The situation is similar when the composition of the injected fluid is slightly less than that of the formation fluid ($\lambda V\beta < 1$) (figure 2*b*). Finally, when the composition of the injection fluid is much less than that of the formation fluid ($\lambda V\beta > 1$), the depletion front outruns the thermal front (figure 2*c*). In this case there is no thermal reaction front. The injection fluid first adjusts to the formation temperature at the thermal front although no reaction takes place here and the fluid remains undersaturated. It then adjusts to the appropriate equilibrium concentration when crossing the depletion front.

If the injection fluid has a lower equilibrium concentration than the formation fluid ($\beta > 1$), two different types of solution can develop as shown in figure 3. First, when the concentration of the injection fluid is slightly less than that of the formation fluid ($\lambda V\beta < 1$), a depletion front develops near the source, upstream of the thermal front (figure 3*a*). Incoming fluid reaches chemical equilibrium (at the injection temperature) across this front. Further downstream, the fluid reaches the thermal front, where it dissolves more of the reactant in the solid matrix in order to retain chemical equilibrium as it changes to the formation temperature. Finally, when the concentration of injection fluid is much less than that of the formation fluid ($\lambda V\beta > 1$), the depletion front outruns the thermal front, and a single reaction front develops downstream of the thermal front (figure 3*b*). In this case, the fluid adjusts to the formation temperature when crossing the thermal front. No reaction takes place here and the fluid remains undersaturated. Subsequently, the fluid attains chemical equilibrium at the formation temperature by crossing the depletion front.

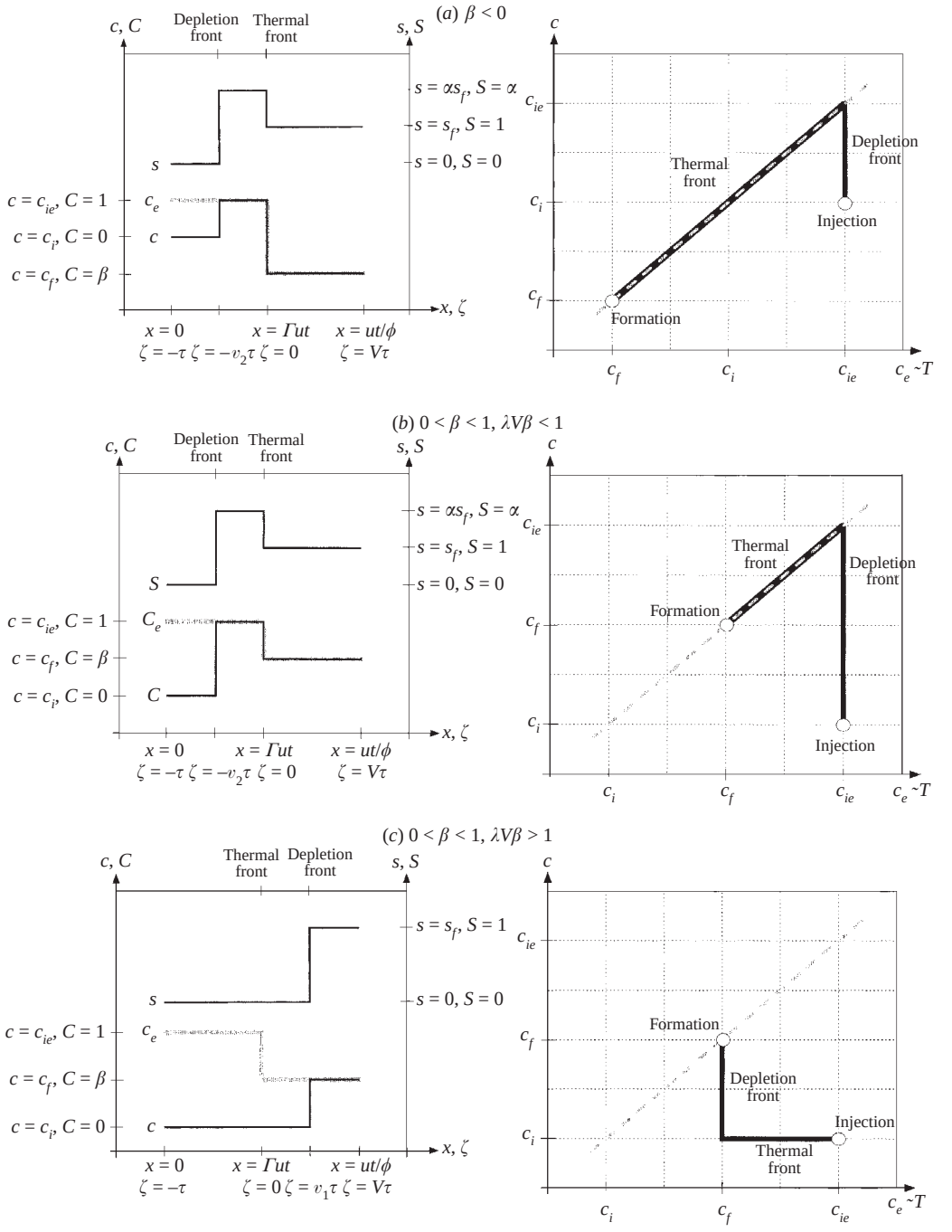

FIGURE 2. The three possible long-time asymptotic regimes when the equilibrium concentration of the injection fluid exceeds that of the formation fluid ($\beta < 1$). This occurs when hot fluid displaces cold (in the case of a prograde mineral) or when cold fluid displaces hot (in the case of a retrograde mineral). The diagrams on the left show the solution profiles. The diagrams on the right show the path of a fluid particle (solid line) in (c_e, c)-space from the point of injection to the final equilibrium downstream of the reaction fronts. The dotted line represents equilibrium.

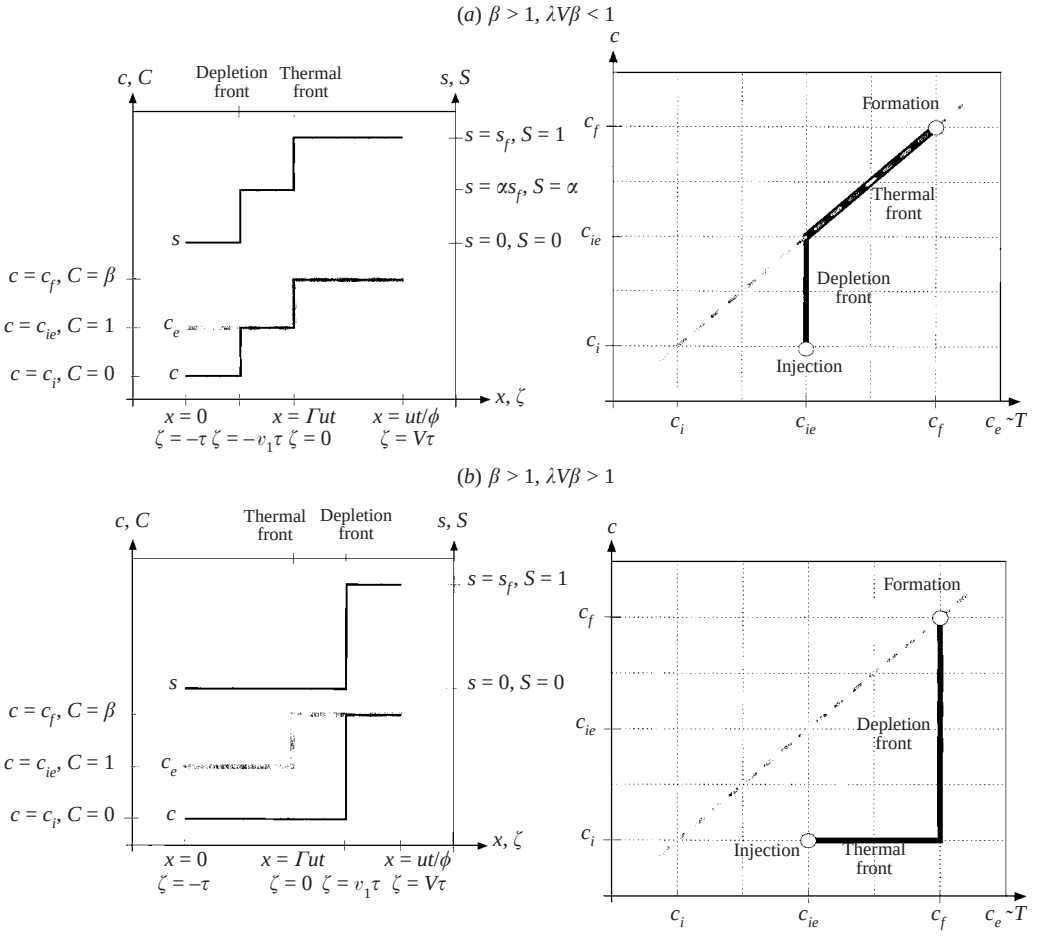

FIGURE 3. As figure 2, but showing the two possible long-time asymptotic regimes when the equilibrium concentration of the formation fluid exceeds that of the injection fluid ($\beta > 1$). This occurs when cold fluid displaces hot fluid (in the case of a prograde mineral) or when hot fluid displaces cold fluid (in the case of a retrograde mineral).

5. Evolution of the system towards asymptotic solutions

The analysis above captures the variety of reaction front structures which may develop at long times as fluid is injected into a formation. We now examine how the system approaches these asymptotic solutions by considering the dimensionless timescales over which the various structures in the asymptotic solutions form.

The timescale over which the depletion front becomes established can be defined as the timescale over which $S \to 0$ at the injection point $\zeta = -\tau$. It then follows from equations (3.3) and (3.7) that the depletion front becomes established when $\tau \sim 1/\lambda\beta P$ in the case of a single front and when $\tau \sim 1/\lambda P$ in the case of a double front. We argued in § 2.3 that the thermal front becomes established when $\tau \sim 1$. An analogous argument shows that the fluid front becomes established when $\tau \sim \epsilon/(1+V)^2$. The manner in which the system approaches the long-time asymptotic solution depends, therefore, on the relative magnitudes of these timescales. We stress that the appropriate long-time asymptotic solution shown in figures 2 and 3 is

determined by the values of the parameters λ, β and V which quantify compositional differences and frontal speeds. The manner in which the asymptotic solution is approached over time, however, depends on the additional parameters P and ϵ which quantify the rates at which diffusion and reaction operate. For example, the parameter P has been regarded as a constant in this model. If the temperature dependence of the reaction rate were to be included, P would not be constant and the timescale taken to reach the asymptotic solution would change. The asymptotic solution at long times, however, would be unaffected.

5.1. *Numerical simulations*

We now present some numerical solutions of the initial value problem of § 2, to illustrate the different ways in which a given long-time asymptotic solution can be approached. The solutions were calculated using the PDECOL solver package of Madsen & Sincovec (1979) as discussed by Hopkins (1992). This solver uses the method of lines, and a finite-element collocation procedure is used for the spatial discretization. The effects of numerical dispersion were minimized in the simulations by the choice a fine spatial mesh.

The evolution of the system is illustrated for a single reaction front in figure 4 and for a double reaction front in figure 5. In both figures, part (*a*) corresponds to 'slow' reactions ($P < 1$), while part (*b*) corresponds to 'fast' reactions ($P > 1$). In both figures the equilibrium concentration (or equivalently, the temperature) adjusts smoothly towards the analytic solution of equation (3.2). The fluid and solid concentrations evolve in a more complex fashion as the depletion front and the thermal front separate in space.

In figure 4(*a*), the first structure to form is the fluid front when $\tau \sim \epsilon/(1+V)^2 \approx 0.001$ followed by the thermal front when $\tau \sim 1$ and the depletion front when $\tau \sim 1/\lambda\beta P \approx 50$. Consequently, a sharp front in fluid concentration forms at the fluid front before moving towards the depletion front as chemical reactions become significant. In figure 4(*b*), the fluid front again forms when $\tau \sim \epsilon/(1+V)^2 \approx 0.001$ but in this case the depletion front forms over a comparable timescale $\tau \sim 1/\lambda\beta P \approx 0.005$ and so there is no time for a sharp fluid front to form. At very small times, diffusion dominates over advection in equations (2.10) and (2.11). Since $\epsilon < 1$ it follows that the thermal difference between the injection and formation fluids (expressed as a change in equilibrium concentration) propagates further than the chemical difference. Hence, there is a region near the source for which $C > C_E$ at short times. Precipitation occurs and the non-dimensional solid concentration S rises above unity. At longer times, however, advection dominates over diffusion and this precipitated zone is removed by a dissolution reaction. At long times both solutions in figure 4 tend towards the type of asymptotic solution shown in figure 3(*b*).

In figure 5(*a*), the first structure to form is the fluid front when $\tau \sim \epsilon/(1+V)^2 \approx 0.004$ followed by the thermal front when $\tau \sim 1$ and the depletion front when $\tau \sim 1/\lambda\beta P \approx 300$. In contrast, in the case shown in figure 5(*b*), the depletion front forms when $\tau \sim 1/\lambda\beta P \approx 0.03$, and so is well established before the thermal front begins to appear sharp. At long times both solutions in figure 5 tend towards the type of asymptotic solution shown in figure 3(*a*).

The evolution of the system towards the other asymptotic cases shown in figures 2 and 3 is similar to figures 4 and 5 but the details differ owing to the different initial conditions.

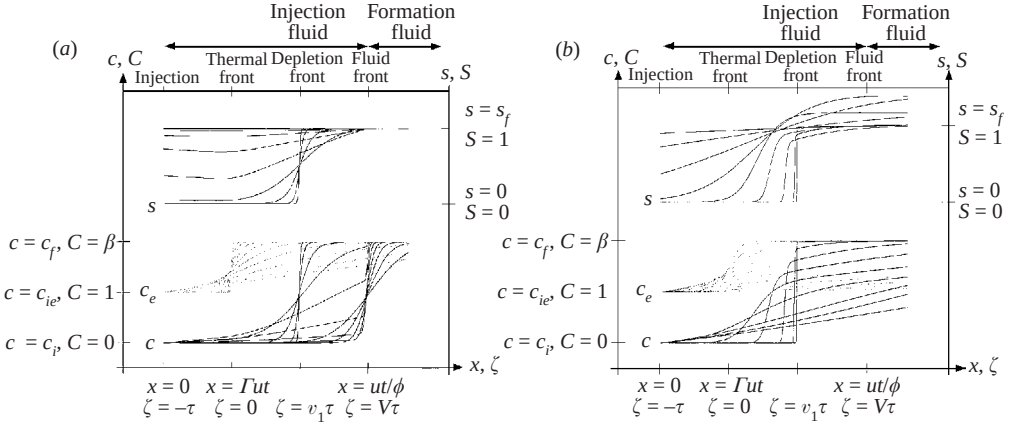

FIGURE 4. Numerical simulations showing the approach to the asymptotic solution in the case of a single reaction front. Parameter values used in this example are: $\lambda = 1$, $\beta = 2$, $V = 2$, and $\epsilon = 0.01$. Hence $v_1 = 1$ and $\omega_1 = P$. (*a*) The evolution of fluid concentration c, equilibrium concentration c_e and solid concentration s when $P = 0.01$. Profiles are shown for $\tau = 0.1, 0.32, 1, 3.2, 10, 32, 100, 320, 1000, 3200, 10\,000$. (*b*) As (*a*) but with $P = 100$, and with profiles shown for $\tau = 0.001, 0.0032, 0.01, 0.032, 0.1, 0.32, 1, 3.2, 10, 32, 100$.

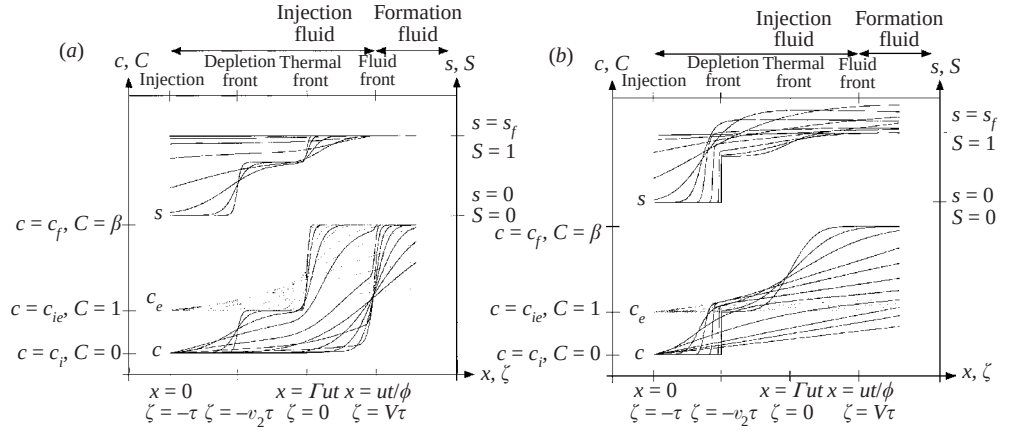

FIGURE 5. The same as figure 4, but for the case of a double reaction front. Parameter values used in this example are: $\lambda = \frac{1}{3}$, $\beta = 3$, $V = \frac{1}{2}$, and $\epsilon = 0.01$. Hence $\alpha = \frac{2}{3}$, $v_2 = \frac{1}{2}$ and $\omega_2 = \frac{2}{3}P$. (*a*) Solution profiles with $P = 0.01$. Profiles are shown at the same dimensionless times as in figure 4(*a*). (*b*) As (*a*) but with $P = 100$. Profiles are shown at the same dimensionless times as in figure 4(*b*).

6. Discussion and conclusions

We have examined the structure of the reaction fronts that develop when undersaturated fluid is injected at a constant rate into a reactive porous medium containing fluid at a different temperature. We have shown that there is a critical difference in composition between the injection and formation fluids which determines whether (i) a single reaction front develops, as a depletion front travels downstream

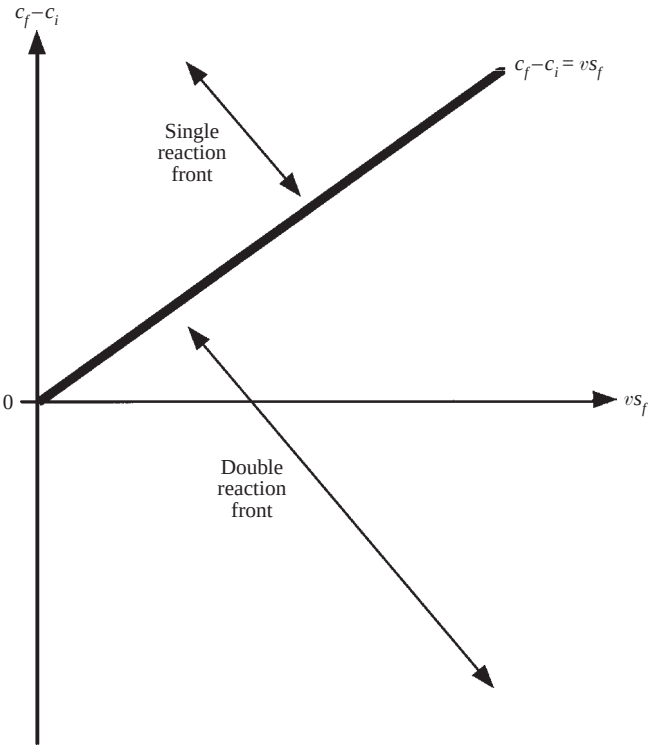

FIGURE 6. Graphical representation of the criterion distinguishing the single and double reaction front solutions. The typical case where $\Gamma = 1$ is shown. $c_f - c_i$ is a measure of the difference in composition between the formation and injection fluids. vs_f is a measure of the amount of solid reactant present initially on the rock.

of the thermal front, or (ii) two distinct reaction fronts evolve, as a separate thermal reaction front propagates downstream of the depletion front. Numerical solution of the initial value problem illustrates how the solution evolves with time (figures 4 and 5) towards the asymptotic reaction front structure (figures 2 and 3). One striking feature of this analysis is that we have identified circumstances in which an initially homogeneous permeable rock may develop three regions of different mineral content as a result of being flooded by fluid with different mineral content and temperature to the original formation fluid (§ 3.2). In other situations, however, we have shown that only two zones of different mineral content develop following the fluid migration through the layer (§ 3.1).

Although the model is simple, it is of interest to examine the implications of this work for the injection of water into hydrocarbon and geothermal reservoirs. First, inequality (3.6) identifies the conditions under which a single reaction front structure develops, depending on the composition of the injected fluid and the initial concentration of reactant in the rock. For a typical system with $\Gamma \sim 1$ this relation reduces to the requirement that $vs_f < c_f - c_i$ for the single reaction front solution to develop. Thus, as shown in figure 6, the single reaction front solution develops when (i) the rock contains relatively little reactant initially, or (ii) the formation fluid has a concentration sufficiently greater than that of the injection fluid. Conversely, a double reaction front solution develops when (i) the rock contains a relatively large amount

of reactant initially, or (ii) the formation fluid has a concentration which exceeds that of the injection fluid by a relatively small amount, or (iii) the injection fluid has a higher concentration than the formation fluid.

The timescale required to establish the reaction structure ($\max(1/k, D_T/\Gamma^2 u^2)$) depends on the effective thermal diffusivity ($D_T \sim 10^{-6}\,\mathrm{m^2\,s^{-1}}$), the speed of the flow ($u \sim 10^{-4}$–$10^{-5}\,\mathrm{m\,s^{-1}}$ for engineering flows), and the reaction kinetics timescale $1/k$ which may be of order tens of minutes to a few hours, although this may vary substantially depending on the conditions. Therefore, for engineering flows we expect the asymptotic reaction front structure of figures 2 and 3 to develop within hours. In the naturally occurring geological context, typical flow rates may be smaller, of order 10^{-6}–$10^{-7}\ \mathrm{m\,s^{-1}}$. The formation of the thermal front then requires about a year, but subsequently the frontal structure of figures 2 and 3 will again provide an accurate asymptotic model for the structure of the reaction fronts.

In the analysis above we have neglected any cross-flow heat transfer to neighbouring impermeable layers. Such layers may be important over long timescales, as the high-permeability aquifer equilibrates thermally through cross-flow diffusion of heat. If the formation consists of a series of impermeable layers with thicknesses of order d, and high-permeability aquifers with thicknesses of order h, then thermal equilibration requires a time of order $t_e \sim (d+h)^2/4D_T$. Therefore, for small times $t \ll t_e$, the value of Γ used in the above model for determining the relative speed of depletion and thermal fronts is that associated with the high-permeability aquifer. However, at longer times, $t \gg t_e$, Γ should take the revised value $\hat{\Gamma} = \rho c_{pl}/(\hat{\phi}\rho_l c_{pl} + (1-\hat{\phi})\rho_s c_{ps})$ where $\hat{\phi} = \phi h/(h+d)$. In this long-time limit, the thermal front migrates at a speed that is smaller than at short times. Therefore, it may be that during the initial phase of injection, a double front structure develops, with the depletion front trailing the thermal reaction front. However, as the aquifer equilibrates with the neighbouring impermeable layers, the thermal reaction front decelerates, and if $\hat{\Gamma}$ is sufficiently small, then the thermal reaction front may be overtaken and incorporated into the depletion front at long times. The effects of such cross-flow diffusion may be important in a highly stratified formation, with relatively thin layers. For example, the time for thermal equilibration across a 1 m layer is of order 0.03 year, while the time for equilibration across a 10 m layer is of order 3 years. The former timescale may be relevant for engineering water injection systems, while the latter may be short in comparison with a natural geologically driven flow. We deduce that the record of a double reaction front in the rock, which may be manifested by the formation of three zones of different mineral content, may be rather different for flows which are relatively short-lived (compared to the thermal equilibration time t_e) and for flows which are relatively long-lived.

Depletion fronts and thermal reaction fronts may produce a substantial change in the permeability of a rock, thereby modifying the flow pattern and pressure drop across the formation with time (Phillips 1991; Raw & Woods 1999). Furthermore, in the case of dissolution, the reaction fronts may become unstable and a broader reaction zone may then develop (cf. Hinch & Bhatt 1990). We plan to report on these effects, as applied to the double reaction front structure, in more detail in a subsequent contribution.

This work has been supported by the BP Institute and the Newton Trust, Cambridge.

Appendix. General recurrence relations

In general, the relationships between the functions in equation (3.16) are

$$f_n = \frac{-\frac{1}{2}Vf'_{n-1} + \frac{1}{2}\eta f'_{n-2} + \frac{1}{4}\epsilon f''_{n-2} - \sum_{m=1}^{n-1} f_m g_{n-m} + \frac{1}{2}(n-2)f_{n-2}}{Pg_0}, \tag{A 1}$$

$$g'_n = -(n-1)(g_{n-1} + \lambda f_{n-1}) - \eta(g'_{n-1} + \lambda f'_{n-1}) - \tfrac{1}{2}\lambda\epsilon f''_{n-1} + \lambda V f'_n, \tag{A 2}$$

for $n \geqslant 0$, where we define $f_m(\eta) = g_m(\eta) \equiv 0$ for $m < 0$. For example, we have

$$f_0(\eta) = 1 + (\beta - 1)\frac{1 + \mathrm{erf}(\eta)}{2}, \tag{A 3}$$

$$g_0(\eta) = 1 + \lambda V(1-\beta)\frac{1 - \mathrm{erf}(\eta)}{2}, \tag{A 4}$$

$$f_1(\eta) = \frac{V(1-\beta)}{2P\sqrt{\pi}}\frac{\exp(-\eta^2)}{g_0(\eta)}. \tag{A 5}$$

It follows that the dimenionless rate of transfer of reactant is, to leading order in $\tau^{-1/2}$,

$$PS(C_E - C) = \tau^{-1/2}\left[\frac{V(1-\beta)}{2\sqrt{\pi}}\right]\exp(-\eta^2). \tag{A 6}$$

REFERENCES

Bowers, T. S., Jackson, K. J. & Helgeson, H. C. 1991 *Equilibrium Activity Diagrams*, pp. 308–349. Springer.

Fayers, F. J. 1962 Some theoretical results conecrning the displacement of a viscous oil by a hot fluid in a porous medium. *J. Fluid Mech.* **13**, 65–76.

Hinch, E. J. & Bhatt, B. S. 1990 Stability of an acid front moving through porous rock. *J. Fluid Mech.* **212**, 279–288.

Hopkins, T. 1992 Remark on "Algorithm 540: PDECOL, General Collocation Software for Partial Differential Equations [D3]". *ACM Trans. Math. Software* **18**, 343–344.

Karakas, M., Saneie, S. & Yortsos, Y. 1986 Displacement of a viscous oil by the combined injection of hot water and a chemical additive. *SPE Res. Engng* July 1986, 391–402.

Lasaga, A. C. 1984 Chemical kinetics of water-rock interactions. *J. Geophys. Res.* **89**, 4009–4025.

Lasaga, A. C. 1998 *Kinetic Theory in the Earth Sciences*. Princeton University Press.

Madsen, N. K. & Sincovec, R. F. 1979 Algorithm 540: PDECOL, General Collocation Software for Partial Differential Equations [D3]. *ACM Trans. Math. Software* **5**, 326–351.

Manning, C. E. 1994 The solubility of quartz in H2O in the lower crust and upper mantle. *Geochim. Cosmochim. Acta* **58**, 4831–4839.

Nordstrom, D. K. & Munoz, J. L. 1994 *Geochemical Thermodynamics*. Blackwell.

Ogata, A. & Banks, R. B. 1961 A solution of the differential equation of longitudinal dispersion in porous media. *USGS Prof. Paper* 411-A.

Ortoleva, P., Merino, E., Moore, C. & Chadam, J. 1987 Geochemical self-organization I: Reaction-transport feedback and modeling approach. *Am. J. Sci.* **287**, 979–1007.

Phillips, O. M. 1990 Flow-controlled reactions in rock fabrics. *J. Fluid Mech.* **212**, 263–278.

Phillips, O. M. 1991 *Flow and Reactions in Permeable Rocks*. Cambridge University Press.

Raw, A. S. & Woods, A. W. 1999 Gravity driven reactions in a porous layer. *Stanford Geothermal Workshop Procedings.*

Woods, A. W. & Fitzgerald, S. D. 1993 The vaporization of a liquid front moving through a hot porous rock. *J. Fluid Mech.* **251**, 563–579.

deZabala, E. F. & Radke, C. J. 1986 A nonequilibrium description of alkaline waterflooding. *SPE Res. Engng* January 1986, 29–48.

deZabala, E. F., Vislocky, J. M., Rubin, E. & Radke, C. J. 1982 A chemical theory for linear alkaline flooding. *SPE J.* April 1982, 199–216.